

A symmetric binary-vortex street behind a longitudinally oscillating cylinder

By S. J. XU^{1,2}, Y. ZHOU^{1†} AND M. H. WANG³

¹Department of Mechanical Engineering, The Hong Kong Polytechnic University Hung Hom, Kowloon, Hong Kong

²School of Aerospace, Tsinghua University, PR China, 100084

³State key Laboratory for Turbulence and Complex System Peking University, Peking, PR China, 100871

(Received 30 November 2003 and in revised form 14 November 2005)

The wake of a streamwise oscillating circular cylinder has been experimentally investigated over a range of oscillation amplitude and frequency ratios using laser-induced-fluorescence flow visualization, particle image velocimetry and hot-wire techniques. Five typical flow structures, referred to as S-I, S-II, A-I, A-III and A-IV, are identified. Special attention is given to the S-II mode because this flow structure is observed experimentally for the first time. It consists of two rows of binary vortices symmetrically arranged about the centreline of the wake. Each binary vortex contains two counter-rotating vortices shed from the same side of the cylinder. This flow structure corresponds to zero mean and fluctuating lift on the cylinder, which could be of engineering significance. A theoretical analysis for this flow has been conducted based on the governing equations. The solution to the two-dimensional vorticity equation suggests that the flow may be considered to be the superposition of two components, i.e. that due to a stationary cylinder in a steady uniform cross-flow and to a cylinder oscillating in fluid at rest, which are characterized by alternate and symmetric vortex shedding, respectively. The solution provides insight into the formation of the various modes of the flow structure. A semi-empirical prediction of the S-II mode structure is developed, which is in excellent agreement with experimental data as well as with previous numerical results.

1. Introduction

When a cylinder is forced to oscillate in a fluid, vortex shedding is influenced by movement-induced control (Naudascher 1987), which is largely dependent on the combination of A/d and f_e/f_s (Karniadakis & Triantafyllou 1989), where f_e is the excitation frequency and f_s is the natural vortex shedding frequency of a stationary cylinder, and A and d are the oscillation amplitude and the diameter of the cylinder, respectively. Since the wake of an oscillating structure is frequently seen in engineering applications, it is of both fundamental and practical significance to investigate how the wake of an oscillating cylinder behaves.

Previous studies have mostly focused on the transverse oscillation of one or more cylinders, perhaps because the lift force on a structure is in many such cases, e.g. an isolated cylinder case, one order of magnitude larger than the drag force (e.g. Griffin & Ramberg 1976; Chen 1987; Williamson & Roshko 1988; Staubli & Rockwell 1989;

† Author to whom correspondence should be addressed: mmyzhou@polyu.edu.hk

Griffin & Hall 1991; Carberry & Sheridan 2001). Subsequently the lateral structural oscillation prevails over that in the streamwise direction. However, the streamwise force can be significant. Structural failure may result from synchronization between the fluid excitation force and the system natural frequency in the streamwise direction. Examples include the damage of piling during the construction of an oil terminal on the Humber estuary of England in the 1960s (Griffin & Ramberg 1976) and of a thermocouple in the fast breeder reactor Monju of the Japan Nuclear Cycle Development Institute in 1995 (Okajima *et al.* 2004). The problem of streamwise oscillation could be particularly severe when a lightly damped cylindrical structure is used in liquids of high density such as water, oil and metal at high temperature.

There have been a small number of experimental investigations involving a streamwise oscillating cylinder in a cross-flow. Tanida, Okajima & Watanabe (1973) measured the lift and drag force on a streamwise oscillating circular cylinder to study the stability of the oscillation of the cylinder at $A/d=0.14$ and $f_e/f_s=0.5-2.2$. Griffin & Ramberg (1976) visualized the vortex formation around a cylinder oscillating in line with the flow at the onset of 'lock-on'. They investigated f_e/f_s and A/d ranging from 1.74 to 2.2 and 0.06 to 0.12 ($Re \equiv U_\infty d/\nu = 190$, where U_∞ is the free-stream velocity and ν is the fluid kinematic viscosity), respectively. Herein, lock-on refers to the situation where the vortex shedding frequency coincides with that of the structural oscillation. An antisymmetric vortex street occurred at $A/d=0.06-0.1$ and $f_e/f_s=1.74-2.2$. As A/d was increased to 0.12, they observed a vortex street consisting of one row of single vortices and one row of counter-rotating vortex pairs. These two different flow structures in effect correspond to A-I and A-III modes, respectively, as categorized by Ongoren & Rockwell (1988), who investigated the flow patterns behind a cylinder oscillating at an angle with respect to the streamwise direction. Their A/d was fixed at 0.13 and 0.3, and f_e/f_s varied from 0.5 to 4.0. Two basic modes, i.e. symmetrical and antisymmetrical vortex formation, were identified. They further classified the two basic modes into five sub-modes: the S mode for the symmetric vortex formation and A-I, II, III, IV modes for the antisymmetric vortex formation. The A-II mode did not occur in the case of a streamwise oscillating cylinder. Recently, Cetiner & Rockwell (2001) studied experimentally forces at the lock-on state on a streamwise oscillating cylinder in flow ($f_e/f_s=0.3-3.0$) and found that the time-dependent transverse force was phase-locked to the cylinder motion and the vortex system occurred both upstream and downstream of the cylinder. These studies have uncovered many important aspects of the physics associated with a streamwise oscillating cylinder wake, but the A/d investigated has so far been relatively small at high oscillation frequencies, i.e. not exceeding 0.3 at $f_e/f_s=1.8$, or when f_e/f_s is low at large A/d , not exceeding 0.44 at $A/d=0.96$. It might be of fundamental interest and also useful for possible future applications to investigate cases at larger A/d and f_e/f_s , even though A/d and f_e/f_s are relatively small in existing engineering applications. Therefore, one question arises: As A/d or f_e/f_s increases, are there any new flow structures other than those summarized in Ongoren & Rockwell (1988)?

The present work aims to study the wake of a streamwise oscillating cylinder, focusing on the case of relatively large A/d and f_e/f_s . The effects of both f_e/f_s and A/d on the wake are investigated. The investigation employs a laser-induced fluorescence (LIF) technique to visualize the flow structure behind the streamwise oscillating cylinder and the qualitative flow images are examined with the quantitative flow field obtained using the particle image velocimetry (PIV). The dominant frequencies in the near wake are examined based on hot-wire data. Dimensional analysis of the

governing equations for the flow is conducted to predict the occurrence of one new flow structure, which is in agreement with experimental observations.

2. Experimental details

2.1. Flow visualization in a water tunnel

The LIF measurements were carried out in a water tunnel, which has a square working section ($0.15\text{ m} \times 0.15\text{ m}$) 0.5 m long. Further details of the tunnel are given in Zhou *et al.* (2001). An acrylic circular tube with a diameter of $d=0.01\text{ m}$ was horizontally cantilever-mounted at the mid-plane of the working section. The gap between the cylinder free end and the wall was about 0.005 m . The cylinder, driven by a microcomputer-controlled DC motor through a linkage, oscillated harmonically in time in the streamwise direction at $A/d=0.5$ and $f_e/f_s=0-3.1$. A detailed description of the cylinder oscillation assembly are given in Lai, Zhou & So (2003). Dye (Rhodamine 6G 99 %) was introduced at the mid-span of the cylinder through two injection pinholes located at 90° , clockwise and anti-clockwise, respectively, from the leading stagnation point. A thin laser sheet, generated by laser beam sweeping, provided illumination over $0 \leq x/d \leq 10$ in the vertical plane through the mid-span of the cylinder. A Spectra-Physics Stabilite 2017 argon ion laser (4W) was used to generate the laser beam and a digital video camcorder was used to record the dye-marked vortex streets at a framing rate of 25 f.p.s. Measurements were carried out for $Re=100$ to 600.

2.2. PIV measurements in a wind tunnel

The PIV measurements were carried out in a closed-loop wind tunnel to obtain both qualitative and quantitative data. The wind tunnel has a square working section ($0.6\text{ m} \times 0.6\text{ m}$) of 2.4 m in length. The viewing window of the working section was made of optical glass in order to maximize the signal-to-noise ratio. The wind speed in the working section can be adjusted from about 0.3 m s^{-1} to 50 m s^{-1} . More details of the tunnel are given in Zhou, Zhang & Yiu (2002) and also Zhou & Yiu (2006).

The cylinder assembly was designed similarly to that used for the LIF measurements. An aluminium alloy tube with a diameter of 0.015 m was cantilever-supported in the horizontal mid-plane of the working section. The length of the cylinder was 0.35 m , thus resulting in a blockage of 1.25% and an aspect ratio of about 23. A 0.15 m long section at the free end of the cylinder was replaced by a transparent acrylic tube in order to allow the laser sheet to shine through, thus minimizing the shadow effects in the PIV measurements. One microcomputer-controlled DC motor system was used to drive the cylinder to oscillate at $A/d=0.5$ to 0.67 and $f_e/f_s=0$ to 1.5 . To minimize the reflection noise generated by the laser sheet shining on the cylinder, the cylinder surface was painted black except for a 0.02 m long section 0.12 m from the free end. In the free stream, the longitudinal turbulence intensity was measured to be approximately 0.4% .

Note that the cylinder in the water tunnel measurements has an aspect ratio of 15. For a stationary cylinder, an aspect ratio of 27 or larger is needed to avoid end effects (King 1977). However, an oscillating cylinder may re-organize vortex shedding to enhance significantly the two-dimensionality of the flow. Griffin (1980) observed that, when A/d was greater than $0.01-0.02$, the correlation coefficient, ρ_p , between spanwise fluctuating pressures increased greatly, compared with a stationary cylinder. For example, given a threshold of $\rho_p=0.5$, the spanwise correlation length was about $1d$ at $A/d=0.025$, $6d$ at $A/d=0.075$ and $10d$ at $A/d=0.125$. For $A/d=0.5$, the

correlation length was estimated to be over $40d$ based on an extrapolation of his data, indicating negligible end effects in the present experiments.

The velocity field was measured using a Dantec standard PIV2100 system. Flow was seeded by smoke that was generated from Paraffin oil of particle size of around $1\ \mu\text{m}$ in diameter. The flow was illuminated in the plane, 0.13 m from the free end of the cylinder, of mean shear by two NewWave standard pulsed laser sources of a wavelength of 532 nm , each having a maximum energy output of 120 mJ . It has been confirmed based on the streamwise mean and root mean square (RMS) velocities (not shown) that the flow was two-dimensional around the plane. Digital particle images were taken using one CCD camera (double frames, 1280×1024 pixels). A Dantec FlowMap Processor (PIV2100 type) was used to synchronize image-taking and illumination. Each image covered an area of $0.115\text{ m} \times 0.092\text{ m}$ of the flow field, i.e. $x/d = 0-7.7d$ and $y/d = -3.1d-+3.1d$; the origin of x and y is defined at the centre of the cylinder. The longitudinal and lateral image magnifications were identical, i.e. 0.09 mm/pixel . Each laser pulse lasted for $0.01\ \mu\text{s}$. The interval between two successive pulses was typically $50\ \mu\text{s}$. Thus, a particle would travel only 0.05 mm (0.56 pixels or $0.003d$) at $U_\infty = 1.0\text{ m s}^{-1}$, at which the PIV measurement was conducted. An optical filter was used to allow only the green wavelength (532 nm) of the laser source to pass through.

Since the cylinder was included in the PIV images, which could cause errors in deriving velocities around the cylinder, it was masked using a built-in masking function in the Dantec PIV2001 system before calculation of particle velocities. In image processing, 32×32 rectangular interrogation areas were used, each area including 32 pixels ($\approx 0.2d$) with 50% overlap with other areas in both the longitudinal and lateral directions. The ensuing in-plane velocity vector field consisted of 79×63 vectors. Approximately the same number of spanwise vorticity component (ω_z) may be obtained based on particle velocities. The spatial resolution for vorticity estimates was about 1.43 mm or $0.095d$. The measurements were conducted at $Re = 1150$.

2.3. Hot-wire measurements

The vortex shedding frequencies in the cylinder wake were measured using two hot wires in the wind tunnel. In order to determine the phase relationship between vortices shed from the two sides of the cylinder, two single hot wires were placed symmetrically at $x/d = 2, 5$ and $y/d = 0, \pm 1, \pm 2, \pm 3, \pm 4$, respectively. Constant-temperature circuits were used for the operation of the hot wires. Experiments were carried out at $Re = 1150$. Signals from the circuits were offset, amplified and then digitized using a 16-channel (12 bit) Analog/Digital board and a personal computer at a sampling frequency $f_{\text{sample}} = 1.5\text{ kHz}$ per channel. The typical duration of each record was about 30 s .

3. Symmetric binary vortex street

The structural oscillation and vortex shedding may or may not be in the lock-on state. The present investigation focused on the lock-on state. The wake of an isolated oscillating cylinder in the lock-on state is dependent on a combination of A/d and f_e/f_s (Karniadakis & Triantafyllou 1989). For $A/d = 0.5-0.67$ and $f_e/f_s = 0-3.1$, five typical flow structures have been identified; their patterns are illustrated, based on the streaklines obtained from LIF flow visualization, in figure 1. Ongoren & Rockwell (1988) reported on four of them (S-I, A-I, A-III and A-IV), though at a different combination of f_e/f_s and A/d . At the higher range of f_e/f_s for the present A/d range,

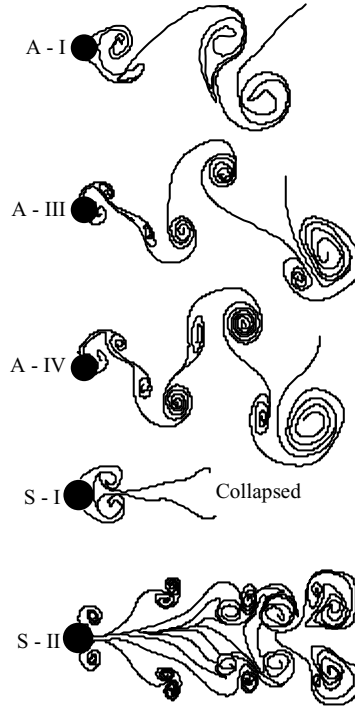


FIGURE 1. Summary of typical flow structures.

a symmetrically formed binary vortex street, referred to as the S-II mode, occurs. This flow is composed of binary vortices, apparently different from the S-I mode flow structure. Each binary vortex comprises two counter-rotating vortices.

Figure 2 presents sequential photographs of various phases in one typical cycle of the cylinder oscillation at $f_e/f_s = 1.74$ and $A/d = 0.5$. A clockwise rotating vortex A_1 above the centreline forms as a result of natural vortex shedding when the cylinder moves opposite to the flow direction (figures 2a–2c). As the cylinder moves from $-A$ to $+A$ in the same direction as the flow (figures 2c–2e), the fluid near the cylinder wall moves with the cylinder under the action of viscosity, but the fluid further away moves in the opposite direction (right to left) relative to the cylinder. The maximum moving velocity of the cylinder is about 5.03 cm s^{-1} ($f_e = 1.6 \text{ Hz}$), while that of water is 4.5 cm s^{-1} . Thus, the maximum relative velocity between water and the cylinder is 0.53 cm s^{-1} , resulting in an instantaneous Reynolds number (based on 0.53 cm s^{-1} and d) of 58. This exceeds the critical Reynolds number (≈ 40 , e.g. Schlichting & Gersten 2000) for vortex shedding. Therefore, a vortex A_2 , of the anticlockwise sense, begins to form. Eventually, the structure containing the pair of counter-rotating vortices A_1 and A_2 separates from the cylinder (figures 2c–2e) and evolves downstream. At the same time, the counter-rotating vortices B_1 and B_2 form another binary vortex and separate from the lower side of the cylinder.

The symmetric binary vortex street is also observed at a higher frequency ratio, up to a maximum $f_e/f_s = 3.08$ (figure 3, $Re = 500$). Note that the increase in f_e/f_s appears to cause a transition from a laminar (figure 2) to turbulent state (figure 3). This observation is consistent with Zdravkovich's (1997) suggestion that, as the oscillation of a cylinder exceeds the threshold amplitude, the oscillation amplitude

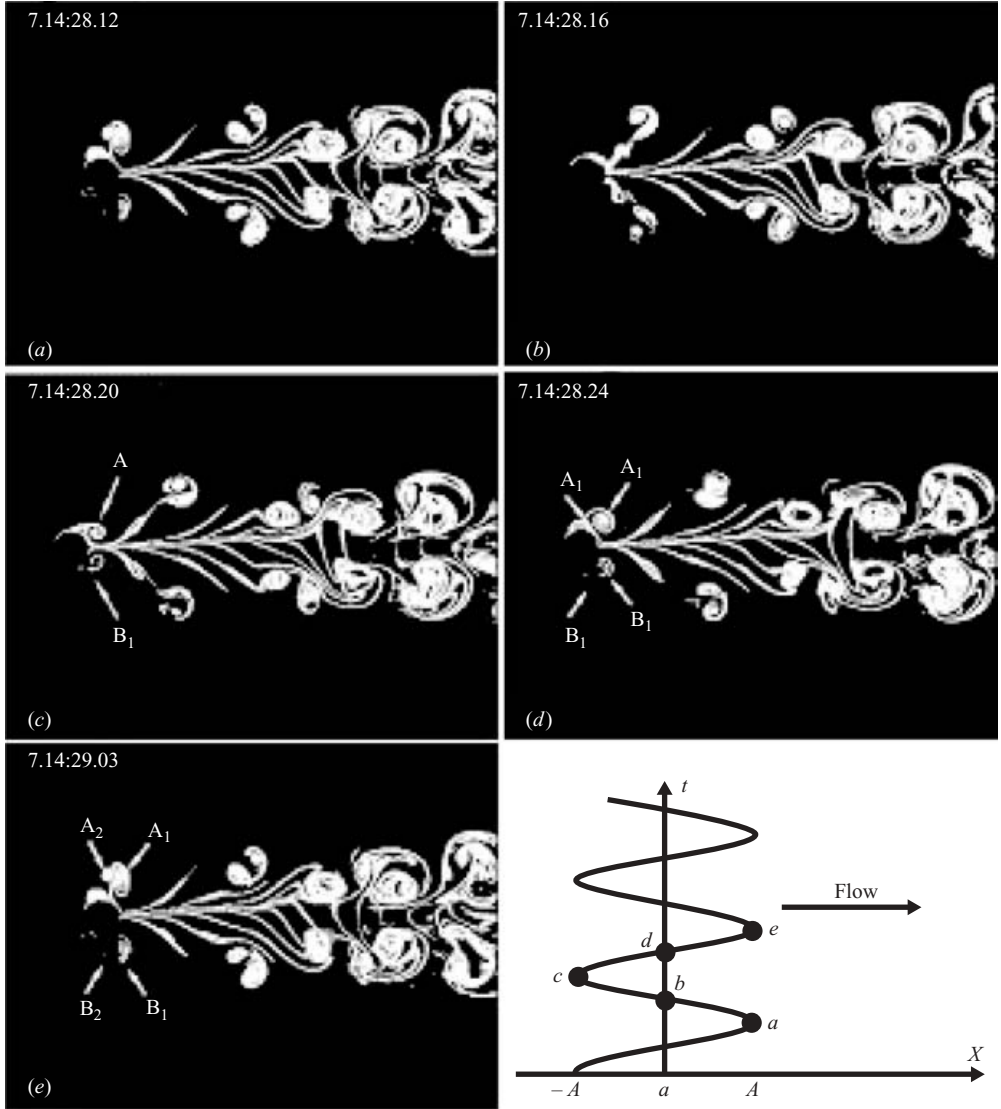


FIGURE 2. Sequential photographs of a symmetric binary vortex street at $f_e/f_s = 1.74$, $Re = 500$ and $A/d = 0.5$.

and frequency may become the controlling parameters of the flow regime within a certain range of the free-stream velocity, instead of Re .

The flow structure is further evident in instantaneous vorticity contours $\omega_z^* = \omega_z d / U_\infty$ (figure 4) obtained from the PIV measurements at $A/d = 0.67$, $Re = 1150$ and $f_e/f_s = 1.45$. Unless otherwise stated, the asterisk denotes normalization by d and U_∞ in this paper. In figure 4(a), the cylinder motion is right to left, generating clockwise (A_{21}) and anti-clockwise (B_{21}) rotating vortices above and below the centreline, respectively, which correspond to vortices A_1 and B_1 in figure 2, respectively. In figure 4(b), the cylinder moves left to right. Two binary vortices, i.e. A_{21} – A_{22} and B_{21} – B_{22} , are shed simultaneously from the upper and lower side of the cylinder, as observed from the LIF data (figure 2). The ω_z^* contours indicate that in the

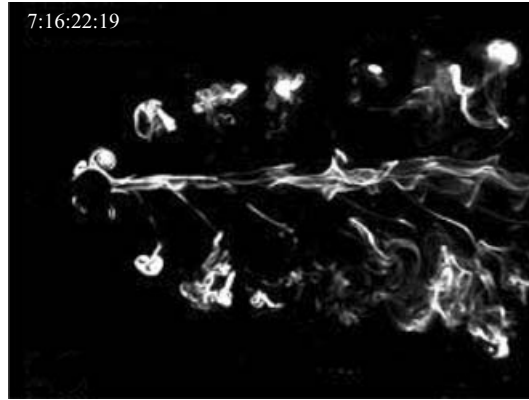


FIGURE 3. The symmetric binary vortex street at $f_e/f_s = 3.1$, $Re = 500$ and $A/d = 0.5$.

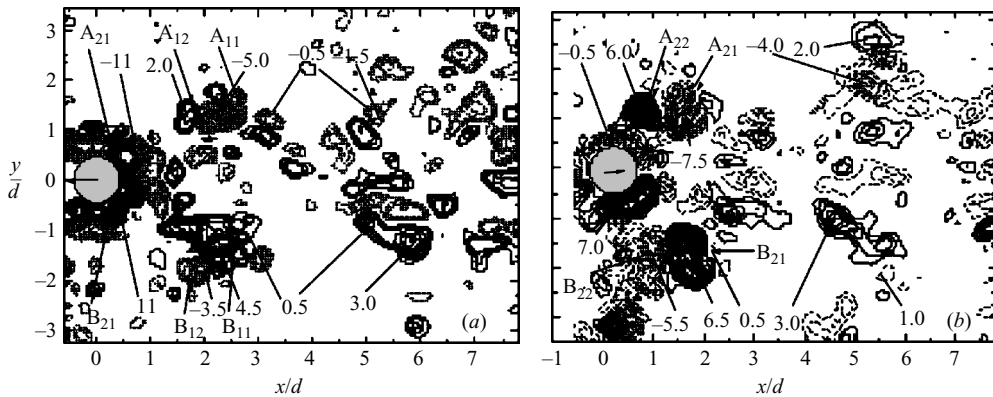


FIGURE 4. Instantaneous vorticity contours $\omega_z^* = \omega_z d / U_\infty$ obtained from the PIV measurement (the contour increment = 0.5, $A/d = 0.67$, $Re = 1150$ and $f_e/f_s = 1.45$). Flow is left to right. (a) The cylinder moves right to left. (b) The cylinder moves left to right.

binary vortex A_{21} (or B_{21}) originating from natural vortex shedding has strength slightly stronger than A_{22} (or B_{22}), generated due to cylinder oscillation. The binary vortices appear relatively short-lived and are barely identifiable for $x/d > 5$. This is in qualitative agreement with the LIF data in the turbulent state (c.f. figure 3) and could be largely attributed to a more meandering motion of vortices in a turbulent state, thus accelerating vorticity cancellation between the counter-rotating vortices in a binary vortex.

The frequency of binary-vortex shedding is identical to that of oscillation. This is evident in the power spectral density function (figure 5) of the hot-wire signal measured at $x/d = 2$ for the same conditions as the PIV measurements, which displays one pronounced peak at $f/f_e = 1$ across the wake. The spectral phase (not shown) between the signals from the two symmetrically arranged hot wires is about zero at $f/f_e = 1$, re-confirming the symmetrical arrangement of binary vortices (figures 3 and 4). Another less pronounced peak occurs at $f/f_e = 2$, which is only discernible when the hot wire is placed far away from the centreline ($y/d = 3$), consistent with the lateral location (figure 3) of the binary vortex in a turbulent state. The peak at

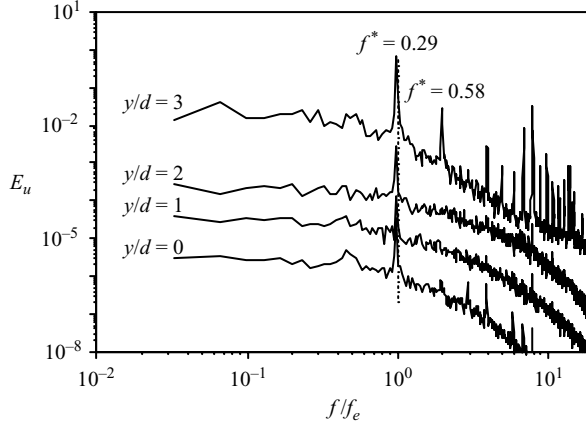


FIGURE 5. Power spectral density function of hot-wire signals obtained at $x/d=2$. $A/d=0.67$, $f_e/f_s=1.45$ and $Re=1150$.

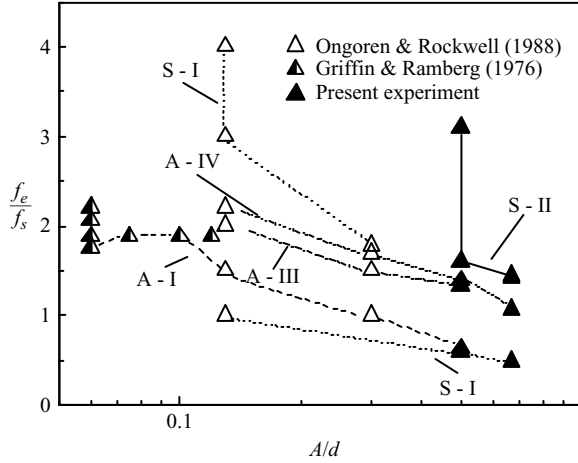


FIGURE 6. Dependence of the flow structure on f_e/f_s and A/d .

$f/f_e=2$ is therefore probably due to the fact that each binary vortex includes two vortices.

4. Effect of frequency and amplitude ratios

4.1. Dependence of the flow structure on f_e/f_s and A/d

Figure 6 presents a collection of experimental data available in the literature and those obtained here. Evidently, the mode of a flow structure depends on both f_e/f_s and A/d . For example, the flow structure of the A-I mode occurs at $f_e/f_s=1.76$ to 2.2 for $A/d=0.06$ (Griffin & Ramberg 1976) and at $f_e/f_s=1.0$ to 1.5 for $A/d=0.12$ or 0.13 (Ongoren & Rockwell 1988). However, the present data show the occurrence of the A-III mode at $f_e/f_s \approx 1.3$ for $A/d=0.5$ and the S-II mode for $f_e/f_s \geq 1.6$ and $A/d=0.5$. In general, for a larger A/d , f_e/f_s is smaller for a particular flow structure mode to start to occur. For a fixed A/d , the S-I mode occurs at the lowest f_e/f_s ,

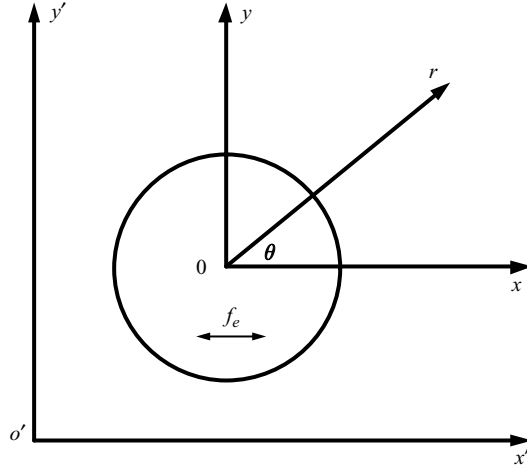


FIGURE 7. Moving reference frame fixed on the cylinder.

followed by the A-I, A-III and A-IV modes as f_e/f_s increases. The S-II mode occurs at the highest f_e/f_s among the five modes.

4.2. Theoretical considerations

4.2.1. Vorticity dynamics on the cylinder

Vortices, as seen in e.g. figure 2, are created on the surface of the cylinder. The origin of vorticity is the cylinder surface, moving with respect to fluid, under the effect of viscosity and the no-slip condition (e.g. Wu & Wu 1989). In this subsection, we attempt to understand the generation of the different flow structures, discussed in §3, based on vorticity dynamics on the cylinder surface.

Consider a moving cylindrical coordinate system, which is fixed on the oscillating cylinder as shown in figure 7. The incompressible Navier–Stokes equations and continuity equation can be written, respectively, as

$$\frac{\partial \mathbf{V}}{\partial t} + \mathbf{V} \cdot \nabla \mathbf{V} = -\frac{1}{\rho} \nabla p + \nu \nabla^2 \mathbf{V} - \mathbf{a}, \quad (4.1a)$$

$$\text{and } \nabla \cdot \mathbf{V} = 0, \quad (4.1b)$$

where \mathbf{V} is the flow velocity vector, p is pressure, ρ is the fluid density, t is time and \mathbf{a} is the acceleration vector of the cylinder. The vorticity equation is given by

$$\frac{\partial \boldsymbol{\omega}}{\partial t} + (\mathbf{V} \cdot \nabla) \boldsymbol{\omega} - (\boldsymbol{\omega} \cdot \nabla) \mathbf{V} = \nu \nabla^2 \boldsymbol{\omega} - \nabla \times \mathbf{a}, \quad (4.1c)$$

where $\boldsymbol{\omega} = \nabla \times \mathbf{V}$ is the vorticity vector.

The cylinder displacement may be written as $X(t) = A \cos(2\pi f_e t + \varphi_0)$, where φ_0 is the initial phase angle of the oscillating cylinder. The maximum velocity of the cylinder occurs at $X=0$:

$$\dot{X}_{\max} = \pm 2\pi f_e A, \quad (4.2)$$

where the positive and negative signs correspond to the cylinder movement along and opposite to the flow direction, respectively. It follows that the cylinder acceleration

$$a = \ddot{X}(t) = -4\pi^2 f_e^2 A \cos(2\pi f_e t + \varphi_0).$$

Let us consider a flow of low Reynolds number, which is approximately two-dimensional around the cylinder. Thus, (4.1a, b, c) can be reduced to

$$\begin{aligned} & \frac{\partial V_r}{\partial t} + V_r \frac{\partial V_r}{\partial r} + \frac{V_\theta}{r} \frac{\partial V_r}{\partial \theta} - \frac{V_\theta^2}{r} \\ &= -\frac{1}{\rho} \frac{\partial p}{\partial r} + \nu \left(\nabla^2 V_r - \frac{V_r}{r^2} - \frac{2}{r^2} \frac{\partial V_\theta}{\partial \theta} \right) + 4\pi^2 f_e^2 A \cos(2\pi f_e t + \varphi_0) \cos \theta, \end{aligned} \quad (4.3a)$$

$$\begin{aligned} & \frac{\partial V_\theta}{\partial t} + V_r \frac{\partial V_\theta}{\partial r} + \frac{V_\theta}{r} \frac{\partial V_\theta}{\partial \theta} + \frac{V_r V_\theta}{r^2} \\ &= -\frac{1}{\rho r} \frac{\partial p}{\partial \theta} + \nu \left(\nabla^2 V_\theta - \frac{V_\theta}{r^2} - \frac{2}{r^2} \frac{\partial V_r}{\partial \theta} \right) + 4\pi^2 f_e^2 A \cos(2\pi f_e t + \varphi_0) \sin \theta, \end{aligned} \quad (4.3b)$$

$$\frac{\partial V_r}{\partial r} + \frac{V_r}{r} + \frac{1}{r} \frac{\partial V_\theta}{\partial \theta} = 0, \quad (4.4)$$

$$\frac{\partial \omega_z}{\partial t} + V_r \frac{\partial \omega_z}{\partial r} + \frac{V_\theta}{r} \frac{\partial \omega_z}{\partial \theta} = \nu \nabla^2 \omega_z, \quad (4.5)$$

where

$$\nabla^2 = \frac{\partial^2}{\partial r^2} + \frac{1}{r} \frac{\partial}{\partial r} + \frac{1}{r^2} \frac{\partial^2}{\partial \theta^2}, \quad \theta \in (0, \pm\pi).$$

In the cylindrical coordinate system,

$$\omega_z = \frac{\partial V_\theta}{\partial r} + \frac{V_\theta}{r} - \frac{1}{r} \frac{\partial V_r}{\partial \theta}. \quad (4.6)$$

On the cylinder surface, the no-slip condition may be stated as

$$V_r = 0, \quad V_\theta = 0, \quad \frac{\partial V_r}{\partial \theta} = 0, \quad \frac{\partial V_\theta}{\partial \theta} = 0. \quad (4.7)$$

Eliminating the terms related to pressure p in (4.3), considering (4.4), (4.6) and (4.7), and noting $r = d/2$ on the cylinder surface, one may obtain after quite exhaustive algebra the governing equation for vorticity generated on the surface:

$$\nu \nabla^2 \omega_z = \frac{8\pi^2 f_e^2 A}{d} \cos(2\pi f_e t + \varphi_0) \sin \theta. \quad (4.8)$$

In view of the no-slip condition (4.7), the vorticity equation (4.5) on the cylinder surface may be reduced to

$$\frac{\partial \omega_z}{\partial t} = \nu \nabla^2 \omega_z. \quad (4.9)$$

Thus, (4.8) can be rewritten as

$$\frac{\partial \omega_z}{\partial t} = \frac{8\pi^2 f_e^2 A}{d} \cos(2\pi f_e t + \varphi_0) \sin \theta. \quad (4.10)$$

Integrating (4.10) yields the vorticity created at the surface of the oscillating cylinder:

$$\omega_z = \frac{4\pi f_e A}{d} \sin(2\pi f_e t + \varphi_0) \sin \theta + \omega_{z,c}(\theta) = \omega_{z,u}(t, \theta) + \omega_{z,c}(\theta), \quad (4.11)$$

where

$$\omega_{z,u}(t, \theta) = \frac{4\pi f_e A}{d} \sin(2\pi f_e t + \varphi_0) \sin \theta. \quad (4.12)$$

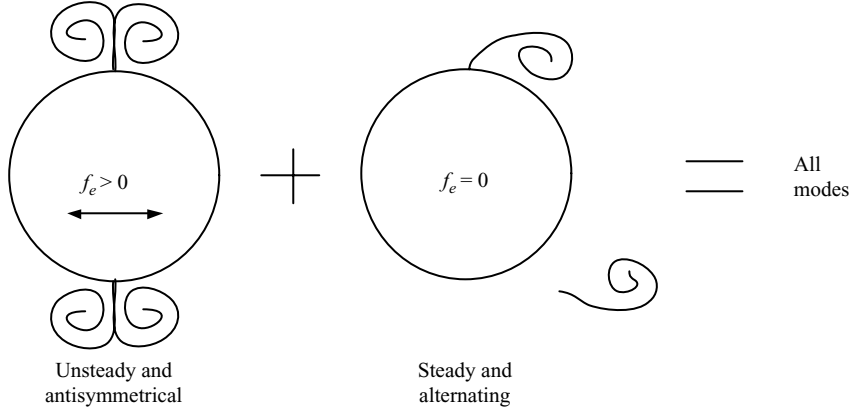


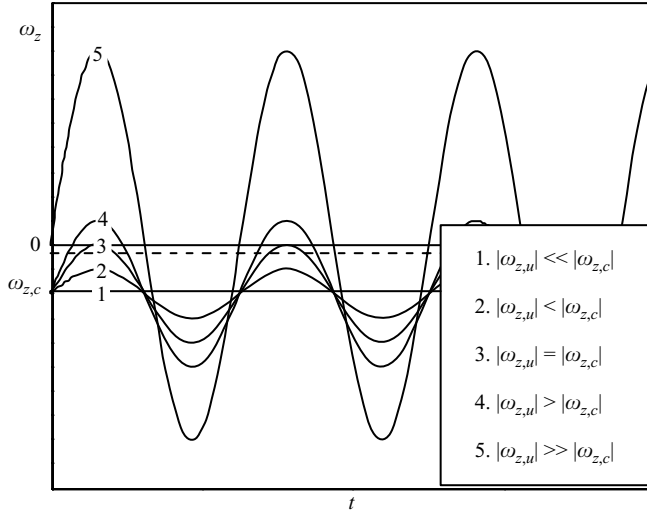
FIGURE 8. Vorticity generated at the cylinder surface.

The distribution of $\omega_{z,u}(t, \theta)$ around the cylinder is antisymmetrical about the x -axis at any instant, and $\omega_{z,c}(\theta)$ is an integral constant, independent of time t and only dependent on θ . Based on the Föppl theorem of total vorticity conservation (Wu & Wu 1996), $\oint \omega_z ds \equiv 0$ around the cylinder surface. It is easy to find $\oint \omega_{z,c} ds \equiv 0$ at any instant; the total vorticity of $\omega_{z,c}(\theta)$ on one side of the x -axis must be identical in magnitude and opposite in sign to that on the other side.

It is evident from (4.11) that, as schematically illustrated in figure 8, the vorticity generated at the cylinder surface comprises two components: (i) an unsteady component, $\omega_{z,u}(t, \theta)$, which is antisymmetrical, or symmetrical in terms of magnitude, about the flow centreline (see 4.12), and (ii) a steady component, $\omega_{z,c}$, which is the solution for the case of a stationary cylinder subjected to a steady uniform cross-flow ($\omega_{z,u}(t, \theta) \equiv 0$). Here, $\omega_{z,u}(t, \theta)$ is dependent on the cylinder oscillation and $\omega_{z,u}(t, \theta) \equiv 0$ for a stationary cylinder. In other words, the vorticity created at the surface of an oscillating cylinder in a uniform flow may be investigated by considering a cylinder oscillating in a fluid at rest plus a stationary cylinder in a steady uniform cross-flow. From the flow stability point of view, the two stabilities or the two components of ω_z compete and interact, which determines the mode of the flow structure. Five combinations of $\omega_{z,u}(t, \theta)$ and $\omega_{z,c}$ are possible and are illustrated in figure 9, namely

(i) When $|\omega_{z,u}| \ll |\omega_{z,c}|$, the cylinder oscillation is negligible; then $\omega_z \approx \omega_{z,c}$, that is, ω_z is approximately independent of time, given by the horizontal line in figure 9 (line 1). The flow structure is the same as that behind a stationary cylinder. At a low Reynolds number, $|\omega_{z,c}|$ is small, $\omega_z \approx \omega_{z,c}$ tends to be symmetric about the x -axis (see the dashed line in figure 9). However, this symmetrical flow mode is unstable and collapses rapidly, as the observed S-I mode (figure 1).

(ii) If the cylinder is forced to oscillate, with $|\omega_{z,u}| < |\omega_{z,c}|$ and $\omega_{z,u}$ appreciable compared with $\omega_{z,c}$ (see line 2 in fig. 9), $\omega_{z,c}$ is predominant and ω_z assumes the sense of $\omega_{z,c}$. Accordingly, the flow should display to a certain degree the features of the Kármán vortex street, showing the A-I mode structure (figure 1). With increasing cylinder oscillation (e.g. increasing f_e/f_s at a fixed A/d), $\omega_{z,u}$ (symmetrical vortex shedding) may compete more vigorously with $\omega_{z,c}$ (alternate vortex shedding), resulting in a different flow structure, i.e. the A-III mode (figure 1). Indeed, the alternate nature of the vortices is discernible for both A-I and A-III modes. However, the A-III mode embraces the vortical structure of twin vortices. More details of the two flow structures can be found in Ongoren & Rockwell (1988b) & Xu (2003).

FIGURE 9. Five combinations of $\omega_{z,u}$ and $\omega_{z,c}$.

(iii) For $|\omega_{z,u}|$ very close to $|\omega_{z,c}|$, $|\omega_{z,u}| \approx |\omega_{z,c}|$ (line 3), a new equilibrium state, namely the A-IV mode, may occur, and ω_z assumes the sense of $\omega_{z,c}$. In this situation, the vortices are rearranged into one staggered binary vortex street. In the first half of one cycle, the upper shear layer around the cylinder separates to form a vortex, which crosses the centreline to join the vortex shed earlier from the lower side of the cylinder, forming one binary vortex in the lower row. A similar process occurs in the other half of the cycle (Xu 2003).

(iv) When $|\omega_{z,u}|$ considerably exceeds $|\omega_{z,c}|$ (line 4), the structure of symmetrically arranged vortices dominates and the stability of the vortex street should be controlled by ω_z . As a result, the S-II mode occurs.

(v) In the limiting case, $|\omega_{z,u}| \gg |\omega_{z,c}|$ (line 5), the flow around the cylinder is only controlled by the cylinder oscillation and steady streaming (Riley 1975) around the cylinder occurs, where the high-frequency oscillation of a cylinder in a fluid initially at rest causes a secondary flow through the action of viscosity in the boundary layer.

The symmetry of the flow structure in cases (iv) and (v) may also be inferred from the boundary vorticity flux, which represents the vorticity that diffuses away from the cylinder surface per unit time and unit area (Lighthill 1963):

$$\sigma = -v \frac{\partial \omega_z}{\partial r} = 4\pi^2 f_e^2 A \cos(2\pi f_e t + \varphi_0) \sin \theta - \frac{2}{d\rho} \frac{\partial p}{\partial \theta}. \quad (4.13)$$

Equation (4.13) can be easily obtained from (4.3b) along with the no-slip condition (4.7). In a situation where the oscillation is very large, that is $f_e A$ is large enough, σ is symmetrical about the x -axis.

4.2.2. Prediction of the S-II mode

The S-II mode is a new finding, displaying a remarkable symmetric binary vortex street. This symmetry implies a negligible mean and fluctuating lift on the cylinder and is potentially of engineering significance. Therefore, it would be interesting to examine the onset conditions of this flow structure. For $U_\infty \neq 0$, the onset of the binary vortex can only occur when $|\omega_{z,u}|$ considerably exceeds $|\omega_{z,c}|$ (line 5 in figure 9). Furthermore, the maximum magnitude, $\omega_{z,u \max}$, of $\omega_{z,u}$ should reach a certain level,

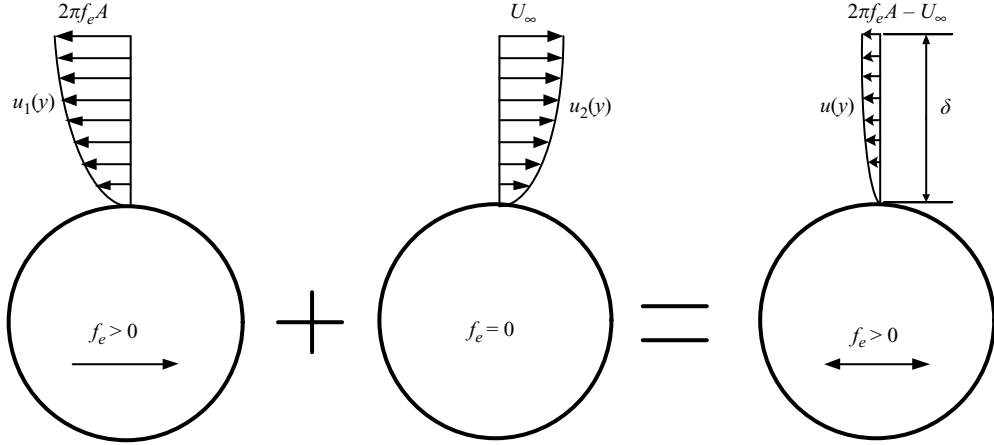


FIGURE 10. The velocity distributions at the top of the oscillating cylinder.

which occurs at $\theta = \pm 90^\circ$, i.e. the top and bottom points of the cylinder, based on (4.12). As discussed earlier, the two vortices of one binary vortex are generated when the cylinder moves oppositely to and in the same direction as U_∞ , respectively. The formation of the binary vortex must be associated with a sufficiently large cylinder velocity (or sufficiently large $\omega_{z,u \max} = 4\dot{X}_{\max}/d$) relative to U_∞ even when the cylinder moves in the same direction as U_∞ . Figure 10 shows schematically the flow velocity distributions, at the top of the cylinder, due to the cylinder oscillation in fluid at rest and a uniform flow over the stationary cylinder, respectively, and the combined velocity $u(y)$. Since $\partial v/\partial x \ll \partial u/\partial y$ (see the Appendix), the vorticity generated is given by

$$\omega_z = \frac{\partial v}{\partial x} - \frac{\partial u}{\partial y} \approx -\frac{\partial u}{\partial y}. \quad (4.14)$$

Hence,

$$\int_0^\delta |\omega_z| dy \approx \int_0^\delta \frac{\partial u}{\partial y} dy = u(\delta) - u(0) = u(\delta),$$

where δ is the boundary layer thickness. Then, the onset condition of the binary vortex may be stated as

$$u(\delta) = 2\pi f_e A - U_\infty > u_c, \quad (4.15)$$

where $u_c > 0$ is the critical velocity at which the vorticity generated in the boundary layer reaches an adequate strength to form a vortex and separates from the cylinder. Relation (4.15) may be rewritten in terms of a relative Reynolds number:

$$\Delta Re = \frac{(2\pi f_e A - U_\infty)d}{\nu} > \frac{u_c d}{\nu} = Re_c, \quad (4.16)$$

where Re_c is the critical Reynolds number.

For a stationary cylinder, $\Delta Re = -U_\infty d/\nu$ is negative and no binary vortex will form since the condition (4.16) cannot be met.

In order to estimate the onset conditions of the binary vortex, Re_c in (4.16) has to be determined. It is well known that for a stationary cylinder the creeping flow regime (no flow separation) occurs for $Re < 5$. For $5 < Re < 40$, the shear layers around the cylinder separate steadily and merge downstream, forming symmetric and steady twin vortices or a closed near wake (e.g. Zdravkovich 1997). For $Re > 40$, unsteady vortex

shedding starts. Once the cylinder is forced to oscillate, the flow is unsteady and the critical Reynolds number for the shear layers to separate from the cylinder in a steady flow becomes invalid. This number should be smaller than 5 in view of the enhanced flow instability. Nevertheless, we will see later that the reduced Re_c has very limited influence on the occurrence of the binary vortex street. For convenience, assume $Re_c = 5$. Condition (4.16) may be reformulated as

$$f_e/f_s \geq \frac{(1 + Re_c/Re)}{2\pi St(Re)} \left(\frac{A}{d}\right)^{-1} = (f_e/f_s)_c, \quad (4.17)$$

where St is the Strouhal number in stationary cylinder case, depending on Re , i.e. $St = St(Re)$, $(f_e/f_s)_c$ is the threshold value for the occurrence of the S-II mode flow structure. The relationship $St = St(Re)$ is well documented in the literature (e.g. Chen 1987; Blevins 1994). Based on (4.17), $(f_e/f_s)_c$ is inversely proportional to A/d , in qualitative agreement with the observation from the experimental data (figure 6) that, as A/d increases, the S-II mode starts to occur at a smaller f_e/f_s . In the limiting case, if $A/d \rightarrow \infty$ (e.g. towing a cylinder through a water tank at some acceleration in the same direction as mean flow), $f_e/f_s \rightarrow 0$; if $A/d = 0$ (a stationary cylinder), $f_e/f_s \rightarrow \infty$, that is, it is impossible to generate the binary vortex. If (4.16) is not satisfied, i.e.

$$\Delta Re = \frac{(2\pi f_e A - U_\infty)d}{\nu} < Re_c,$$

for a small $(2\pi f_e A - U_\infty)$, modes other than the S-II mode flow structure then occur.

For $40 < Re < 200$, $St(Re) = 0.21(1 - 21/Re)$ (Blevins 1994), (4.17) may be written as

$$\frac{f_e}{f_s} \geq \frac{(Re + Re_c)}{0.42\pi(Re - 21)} \left(\frac{A}{d}\right)^{-1} = \left(\frac{f_e}{f_s}\right)_c, \quad 40 < Re < 200 \quad (4.18a)$$

At a large Re , say > 250 , $St(Re) \approx 0.2$, even if we take $Re_c \approx 5$, $Re_c/Re = 5/Re \approx 0$, the Re effect on the occurrence of the S-II mode should be negligible. Equation (4.17) can then be simplified:

$$\frac{f_e}{f_s} \geq \left(\frac{f_e}{f_s}\right)_c \approx \frac{5}{2\pi} \left(\frac{A}{d}\right)^{-1}. \quad (4.18b)$$

Therefore, (4.17) or (4.18) is the condition for the occurrence of the S-II mode.

Figure 11 presents the prediction based on (4.17) together with available experimental data and numerical data obtained from Mittal & Tezdogar (1992) at $Re = 100$ and Sarpkaya *et al.* (1992) at $Re = 800$. The S-II mode flow structure occurs in the region above the curve. The open symbols represent the flow structures of the S-I, A-I, A-III and A-IV modes, while the solid symbols indicate the occurrence of the S-II mode. A number of comments can be made based on the figure. (i) As Re increases at an increment of 50, the curve translates downwards, indicating a dependence of the occurrence of the S-II mode on Re , but the translating increment becomes smaller for higher Re , suggesting a diminishing Re effect, in particular for $Re > 250$. (ii) The predicted occurrence of the S-II mode is in excellent agreement with both experimental and numerical data. For $A/d = 0.5$ and $Re = 100$, the S-II mode is predicted from (4.17) to occur at $f_e/f_s = 1.05/[\pi St(Re)] \approx 0.334/St(100)$, where $St(100)$ represents the Strouhal number at $Re = 100$. This value was $0.35/St(100)$ based on Mittal & Tezdogar's (1992) numerical simulation. Good agreement is also evident between the prediction and Sarpkaya *et al.*'s (1992) numerical data (figure 11). For $A/d = 0.5$ and $Re = 150$, the S-II mode is predicted from (4.17) to occur at $f_e/f_s \approx 1.7$, while it is observed experimentally at $f_e/f_s \approx 1.74$. Considering

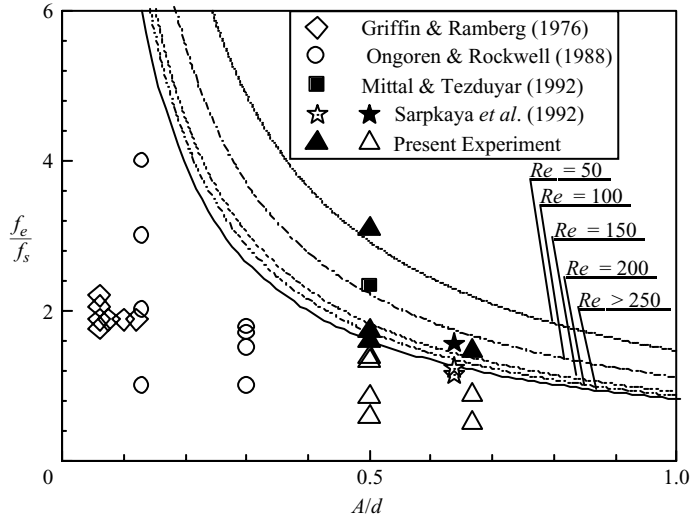


FIGURE 11. Curves show the prediction of the S-II mode flow structure. Solid symbols indicate S-II mode and open symbols represent other modes.

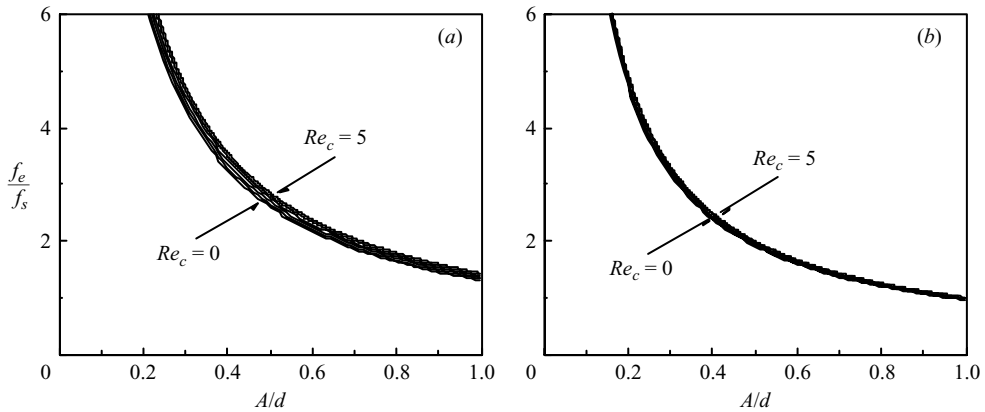


FIGURE 12. Dependence on Re_c of the predicted occurrence of the S-II mode structure: (a) $Re = 50$; (b) $Re = 100$.

the small Re effect on this changeover for $Re \geq 150$, the agreement between previous numerical or present experimental data and the prediction of the occurrence of the S-II mode structure suggests that the choice of the critical Reynolds number ($Re_c = 5$) for the inception of the binary vortex formation is reasonable, which will be explained later. (iii) The occurrence of the S-II mode requires $f_e/f_s > 6.0$ for $A/d = 0.13$, $f_e/f_s > 2.7$ at $A/d = 0.3$, or $f_e/f_s > 0.83$ at $A/d = 0.96$, which may explain why Ongoren & Rockwell (1988) and Cetiner & Rockwell (2001) failed to observe this flow structure (Ongoren & Rockwell's f_e/f_s was up to 4 at $A/d = 0.13$ and did not exceed 1.8 at $A/d = 0.3$. Cetiner & Rockwell's f_e/f_s was 0.3 at $A/d = 0.96$). (iv) Apart from Re , initial conditions such as turbulence level, roughness of cylinder, etc. may affect the value of Re_c and hence the occurrence of the S-II mode.

Equation (4.17) implies an effect of Re_c on the occurrence of the binary vortex street at a small Re . Figure 12 shows the Re_c effect on the predicted result at $Re = 50$

and 100, respectively. At $Re = 50$, the maximum difference in the frequency ratio between the choice of $Re_c = 5$ and 0 is 9%. At $Re = 100$, this difference diminishes to 5%. It may be concluded that the choice of Re_c in the range of 0 and 5 has a negligible effect on the prediction of the S-II mode structure unless $Re \leq 50$. This explains why the prediction with the use of the critical Reynolds number ($Re_c = 5$) for a steady flow in figure 11 agrees with the experimental and numerical data, which were all obtained at $Re \geq 100$.

5. Conclusions

The wake of a streamwise oscillating cylinder has been experimentally investigated using LIF, PIV and hot-wire techniques. The flow structure depends on both f_e/f_s and A/d . Five distinct modes of flow structures have been identified for $f_e/f_s = 0-3.08$ and $A/d = 0.5-0.67$. These modes are designated as S-I, A-I, A-III, A-IV, and S-II.

The flow structure of the S-II mode, consisting of two rows of binary vortices symmetrically arranged about the wake centreline, is systematically and experimentally studied for the first time. Each binary vortex contains two counter-rotating vortices shed from the same side of the oscillating cylinder, in distinct contrast with the counter-rotating vortex pairs of A-III and A-IV modes, which are shed from different sides of the cylinder (Ongoren & Rockwell 1988; Xu 2003). The experimental finding confirms previous numerical results (Mittal & Tezduyar 1992; Sarpakya *et al.* 1992). Being symmetrical about the centreline, the flow structure should correspond to negligible mean and r.m.s. lift coefficients, which may be potentially of engineering significance.

The two-dimensional vorticity equation has been solved for this flow. The solution suggests that the flow may be considered to be the superposition of two components, i.e. a stationary cylinder in a steady uniform cross-flow and a cylinder oscillating in a fluid at rest, which are characterized by alternate and symmetric vortex shedding, respectively. The interactions of the two components determine the mode of the flow structure. The solution provides insight into the formation of the various modes of the flow structure. Based on the analysis of vorticity, a semi-empirical prediction of the S-II mode structure is developed, which is in excellent agreement with experimental data as well as with previous numerical results. The analysis indicates that the critical frequency ratio, $(f_e/f_s)_c$, for the S-II mode to occur is inversely proportional to A/d and depends on Re . However, this Re dependence is negligible for $Re > 250$.

Y. Z. wishes to acknowledge support given to him by the Research Grants Council of the Government of the HKSAR through Grant PolyU 5316/03E.

Appendix. Proof of $\partial v/\partial x \ll \partial u/\partial y$

Consider two points on the cylinder surface at $\theta = \pm 90^\circ$. Use L_x and L_y to denote the longitudinal and lateral characteristic dimensions in the boundary layer, respectively. Apparently, L_y is of the same order as the boundary layer thickness δ . Therefore,

$$L_y \sim \varepsilon L_x, \quad (\text{A } 1)$$

where ε is a small quantity. Noting $\partial u/\partial x + \partial v/\partial y = 0$, one may obtain

$$v \sim \frac{u}{L_x} L_y \sim \varepsilon U_\infty, \quad (\text{A } 2)$$

Therefore,

$$\frac{\partial v}{\partial x} \sim \varepsilon \frac{U_\infty}{L_x} \sim \varepsilon^2 \frac{\partial u}{\partial y}, \quad (\text{A } 3)$$

Equation (A 3) shows that $\partial v/\partial x$ is a very small quantity compared with $\partial u/\partial y$, thus being negligible in the calculation of ω_z at $\theta = \pm 90^\circ$.

REFERENCES

- BLEVINS, D. 1994 *Flow-induced Vibration*. Krieger.
- AIDUN, C. K., LU, Y. N. & DING, E. 1998 *J. Fluid Mech.* **373**, 287–311.
- CARBERRY, J. & SHERIDAN, J. 2001 *J. Fluids Struct.* **15**, 523–532.
- CETINER, O. & ROCKWELL, D. 2001 *J. Fluid Mech.* **427**, 1–59.
- CHEN, S. S. 1987 *Flow-induced Vibration of Circular Cylinder Structures*, pp. 255, 260–263. Hemisphere.
- CHEN, S. & DOOLEN, G. 1998 *Annu. Rev. Fluid Mech.* **30**, 329–364.
- GRIFFIN, O. M. 1980 *NRNRL Mem. Rep.* 4157. Naval Research Laboratory, Washington.
- GRIFFIN, O. M. & RAMBERG, S. E. 1976 *J. Fluid Mech.* **75**, 257–271.
- GRIFFIN, O. M. & HALL, M. S. 1991 *Trans. ASME: J. Fluids Engng* **113**, 526–537.
- HOMSY, G. M., AREF, H., BREUER, K. S. *et al.* 2002 *Multi-Media Fluid Mechanics*. Cambridge University Press.
- KARNIADAKIS, G. E. & TRIANTAFYLLOU, G. 1989 *J. Fluid Mech.* **199**, 441–469.
- KING, R. 1997 *Ocean Engng* **4**, 141–171.
- LAI, W. C., ZHOU, Y. & SO, R. M. C. 2003 *Phys. Fluid*, **15**, 1687–1695.
- LADD, A. J. C. 1994 *J. Fluid Mech.* **271**, 285–309.
- LIGHTHILL, M. J. 1963 Introduction: boundary layer theory. In *Laminar Boundary Layers* (ed. L. Rosenhead), pp. 46–113. Oxford University Press.
- MITTAL, S. & TEZDUYAR, T. E. 1992 *Intl J. Numer. Meth. Fluids* **15**, 1073–1118.
- NAUDASCHER, E. 1987 *J. Fluids Struct.* **1**, 265–298.
- OKAJIMA, A., NAKAMURA, A., KOSUGI, T., UCHIDA, H. & TAMAKI, R. 2004 *Eur. J. Mech. B-Fluids* **23**, 115–125.
- ONGOREN, A. & ROCKWELL, D. 1988 *J. Fluid Mech.* **191**, 225–245.
- RILEY, N. 1975 *J. Fluid Mech.* **68**, 801–812.
- RILEY, N. 2001 *Annu. Rev. Fluid Mech.* **33**, 43–65.
- SARPKAYA, T., PUTZIG, C., GORDON, D., WANG, X. & DALTON, C. 1992 *J. Offshore Mech. Artic Engng* **114**, 219–298.
- SCHLICHTING, H. & GERSTEN, K. 2000 *Boundary Layer Theory*, 8th Edn, pp. 22, 292–365. Springer.
- STAUBLI, T. & ROCKWELL, D. 1989 *J. Fluid Mech.* **203**, 307–346.
- STUART, J. T. 1966 *J. Fluid Mech.* **24**, 673–687.
- TANIDA, Y., OKAJIMA, A. & WATANABE, Y. 1973 *J. Fluid Mech.* **61**, 769–784.
- WILLIAMSON, C. H. K. & ROSHKO, A. 1988 *J. Fluids Struct.* **2**, 355–381.
- WU, J. Z. & WU, J. M. 1996 *Adv. Appl. Mech.* **32**, 119–275.
- WU, J. Z. & WU, J. M. 1989 *J. Fluid Mech.* **254**, 183–211.
- XU, S. J. 2003 Fluid-structure interactions of an oscillating cylinder in cross flow in the presence of a neighbouring cylinder. PhD thesis of the Hong Kong Polytechnic University, pp. 29–32.
- ZDRAVKOVICH, M. M. 1997 *Flow around Circular Cylinders, Vol. 1: Fundamentals*, pp. 6–13.
- ZHOU, Y., WANG, Z. J., SO, R. M. C., XU, S. J. & JIN, W. 2001 *J. Fluid Mech.* **443**, 197–229.
- ZHOU, Y., ZHANG, H. J. & YIU, M. W. 2002 *J. Fluid Mech.* **458**, 303–332.
- ZHOU, Y. & YIU, M. W. 2006 Flow structure, momentum and heat transport in a two-tandem-cylinder wake. *J. Fluid Mech.* **548**, 17–48.